Experimental Investigation of Lens Combinations on the Performance of Vehicular VLC

Bassam Aly*,†, Mohammed Elamassie†, Hossien B. Eldeeb†, and Murat Uysal†
*R&D Department, Ford Otosan, Istanbul, Turkey, 34885.
†Department of Electrical and Electronics Engineering, Özyeğin University, Istanbul, Turkey, 34794.
E-mails: bmohamed@ford.com.tr, mohammed.elamassie@ozu.edu.tr,
hossien.eldeeb@ozu.edu.tr, murat.uysal@ozyegin.edu.tr.

***Abstract*—With the increasing adoption of LEDs in outdoor light sources such as traffic lights, street lights and vehicle headlamps, visible light communication (VLC) has the promise to become a major enabler for vehicle-to-vehicle and vehicle-to-infrastructure communications. In this paper, we experimentally investigate the effect of using different lens combinations on vehicular VLC systems in outdoor environments. First, we measure the effective channel coefficient which includes the effect of both front-ends and propagation channel. Then, based on the estimated channel coefficients, we characterize the vehicular system performance in terms of signal-to-noise ratio and quantify improvements from utilizing different lens combinations.**

***Index Terms*—Visible light communication, vehicular communication, experimental verification.**

I. Introduction

Intelligent transportation systems (ITS) aim to provide safe and comfortable driving [1] and build upon the use of vehicular connectivity. Vehicular communications can be in the form of vehicle-to-vehicle (V2V) and vehicle-to-infrastructure (V2I) commonly abbreviated as V2X [2]. As a potential V2X solution, visible light communications (VLC) was proposed which stands out with its larger bandwidth and its immunity to the interference in comparison to RF-based vehicular technologies [3], [4]. VLC is based on the principle of modulating light emitting diodes (LEDs) without any adverse effect on illumination levels. With the increasing adoption of LEDs in outdoor light sources such as traffic lights, headlamps, and turn-indicator signals, VLC has the promise to become a major enabler for ITSs [5].

Vehicular VLC has attracted some attention in the literature. Earlier works have mainly focused on channel modeling and physical layer designs [6]–[9]. More recent works are experimental in nature and have demonstrated the feasibility of vehicular VLC in outdoor conditions [10]–[13]. In these works, either headlights or taillights of the vehicles are used as transmitters. For example, in [12], using a VW Passat 18W headlight, a packet delivery ratio (PDR) of more than 90% was achieved at distance of 60 m. In another work [13], a data rate of 9.5 Kbps was achieved at distance of 30 m using a red colored taillight. In [14], an experimental set-up with a phosphor-white OSTAR LED was investigated for V2V message delivery using a CAN bus controller for in-car integration. A number of lens combinations was further investigated, but the performance measurements were limited to indoor environments and no actual vehicle was used in the measurements.

In this paper, we experimentally investigate the effect of using different lens combinations on vehicular VLC systems in outdoor environments. First, we obtain the optical channel coefficient of vehicular scenario based on non-sequential ray tracing approach in Zemax® similar to [15], [16] and verify it through measurements. Then, we carry out measurements to obtain the effective channel coefficient which includes the effect of both front-ends and propagation channel. Based on the estimated channel coefficients, we characterize the system performance in terms of signal-to-noise ratio (SNR) for all lens combinations under consideration. The effect of interference from other light sources and the effect of receiver orientation are further discussed.

The rest of the paper is organized as follows: Section II describes the system model. In section III, the experimental set-up is illustrated. Section IV provides the experimental results. Finally, the paper is concluded in Section V.

II. System Model

We consider a vehicular VLC system with on-off keying (OOK). Let $S(i),\ i=1,\cdots,L_{\mathrm{D}}$ denote the i^{th} transmitted OOK symbol where L_{D} is the number of transmitted bits per frame. The signal that drives the LED can be written as [17]

$$x_{\mathrm{LED}}(t)=AG_T\left(\sqrt{P}\sum_{i=1}^{L_D}S(i)\delta(t-iT_s)\right)\otimes p_T(t)+V_{DC}, \quad (1)$$

where $\delta(\cdot)$ is the Dirac delta function, P is the average electrical transmit power, A is an amplification factor, G_T is the lens gain, $p_T(t)$ is the transmit pulse shaping filter, T_s is pulse duration and V_{DC} is the DC bias.

At the receiver front-end side, the light is converted into an electrical signal by a photodetector with responsivity of R. Let $p_R(t)$ and G_R denote, respectively, receiver matched filter and receiver lens gain. The electrical received signal after the photodetector can be written as

$$\begin{aligned}x_{\mathrm{PD}}(t)=&\left(\sqrt{P}\sum_{i=1}^{L_D}S(i)\delta(t-iT_s)\right)\otimes h_{eff}(t)\\&+V_{R_{DC}}+w_g(t),\end{aligned} \quad (2)$$

The work of both Bassam Aly and Hossien Eldeeb was supported by the European Horizon 2020 MSC ITN (VISION) under Grant 764461. The work of M. Uysal was supported by the Turkish Scientific and Research Council (TUBITAK) under Grant 215E311.

where $V_{R_{DC}} = RG_R V_{DC} \otimes l(t) \otimes h(t) \otimes p_R(t)$ and $w_g(t) = w(t) \otimes p_R(t)$. Here, $w(t)$ is additive white Gaussian noise term with zero mean and variance of σ_n^2.

In (2), $h_{eff}(t)$ is the "effective channel impulse response" and defined as $h_{eff}(t) = h_{sys}(t) \otimes h_{opt}(t)$. Here, $h_{sys}(t) = ARG_T G_R p_T(t) \otimes l(t) \otimes p_R(t)$ where $l(t)$ is the combined impulse response of LED and opto-electronic front-end and $h_{opt}(t)$ is the impulse response of propagation channel. Under the assumption that the pulse duration is much larger than delay spread, $h_{eff}(t)$ reduces to a single tap. Therefore, the effective channel coefficient can be simply expressed as $h_{eff} = \int_0^\infty h_{eff}(t)\, dt$. The received signal can be then written as

$$x_{\mathrm{PD}}(i) = \sqrt{P_{\mathrm{t}}}\, h_{eff} S(i) + V_{R_{DC}} + w(i) \cdot \tag{3}$$

At the receiver side, we first perform symbol timing using the maximum output energy method [18, Chapter 5]. Then frame detection is performed in order to resolve multiple symbol period delays. We determine the beginning of the frame by correlating the received signal with the known training sequence for frame detection that is placed at the header of the transmitted frame [19].

For frame detection, DC-bias estimation and channel estimation, a training sequence with a length of L_{TS} is used. It consists of L_{z} zeros and L_{o} ones, i.e., $L_{\mathrm{TS}} = L_{\mathrm{z}} + L_{\mathrm{o}}$. Based on (3), received signals for zeros and ones can be written as $x_{\mathrm{z}}(i) = V_{R_{DC}} + w(i), \quad i = 1, \cdots, L_{\mathrm{z}}$ and $x_{\mathrm{o}}(i) = \sqrt{P_{\mathrm{t}}}\, h_{eff} + V_{R_{DC}} + w(i), i = 1, \cdots, L_{\mathrm{o}}$. $V_{R_{DC}}$ can be simply estimated by taking the average of x_{zeros}, i.e., $\widehat{V_{R_{DC}}} = (1/L_{\mathrm{z}}) \sum_{i=1}^{L_{\mathrm{z}}} x_{\mathrm{z}}(i)$ where $\widehat{w(i)} = \left(V_{R_{DC}} - \widehat{V_{R_{DC}}}\right) + w(i)$. Similarly, noise power and effective channel coefficient can be estimated, respectively, as

$$\widehat{\sigma_n^2} = \frac{1}{L_{\mathrm{z}}} \sum_{i=1}^{L_{\mathrm{zeros}}} \left| x_{\mathrm{z}}(i) - \widehat{V_{R_{DC}}} \right|^2. \tag{4}$$

$$\widehat{h_{eff}} = \frac{1}{\sqrt{P} L_{\mathrm{o}}} \sum_{l=1}^{L_{\mathrm{ones}}} \left(x_{\mathrm{o}}(i) - \widehat{V_{R_{DC}}} \right). \tag{5}$$

Based on (4) and (5), we can define the estimated received SNR as

$$\widehat{SNR} = P \widehat{h_{eff}}^{\,2} \Big/ \widehat{\sigma_n^2}. \tag{6}$$

III. Experimental Set-Up

The block diagram of experimental set-up is illustrated in Fig. 1.a. LabVIEW software generates digital waveform and passes it with Ethernet cable to a modified NI 2920 USRP (with LFTX daughter-board) for digital-to-analogue conversion [20]. Analog signal is transmitted by a custom-design VLC front-end [21] with an integrated LED which has a 60-degree half angle Lambertian pattern. As illustrated in Fig. 1.b, the TX front-end was mounted at a height of 70 cm from the ground (same as front headlight). At the receiver side, a custom-design VLC front-end with 170-degree FOV [21] (mounted on the other vehicle at a height of 55 cm under the taillight) is used. It converts the optical received intensity to an electrical signal. A modified NI 2920 USRP

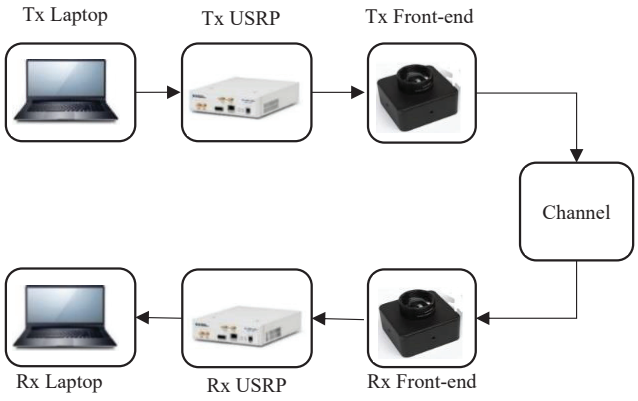

(a)

(b)

Fig. 1. (a) Block diagram of experimental set-up and (b) Pictures taken from experiment.

TABLE I
Experimental Set-Up Parameters

Link distance	d	$0.5, 1, 1.5, \cdots, 5$ m
Average electrical transmitted power	P	0 dB
LED half angle	$\theta_{1/2}$	60°
Power meter reception area	A_r	$\pi\left(6 \times 10^{-3}\right)^2$ m2
Training sequence length for frame detection	L_{FD}	80
Training sequence length for channel estimation	L_{CE}	80
Guard band length	L_G	6
Number of frames	N_F	200
Number of data symbols per frame	L_D	8000 bit/ frame
Up-sampling factor	U	20
USRP sampling rate	f_s	7×10^6 Sample/sec
RRC pulse shaping filter length	L_{PS}	40
Roll-off factor	β	0.5

(with LFRX daughter-board) is used for analogue-to-digital conversion. The rest of the online signal processing is done via LabVIEW on the receive PC. All the experimental set-up parameters are listed in Table I.

To extend the communication distance as well as improve the received SNR, we investigate the use of different lens combinations at both transmitter and receiver side. Plano-convex lenses at transmitter side are used to collimate the light pattern. At the receiver side, plano-convex and biconvex lenses are selected to reduce the photodetector FOV and consequently enhance the receive SNR at further distances. As illustrated in Fig. 2, we consider four different combinations:

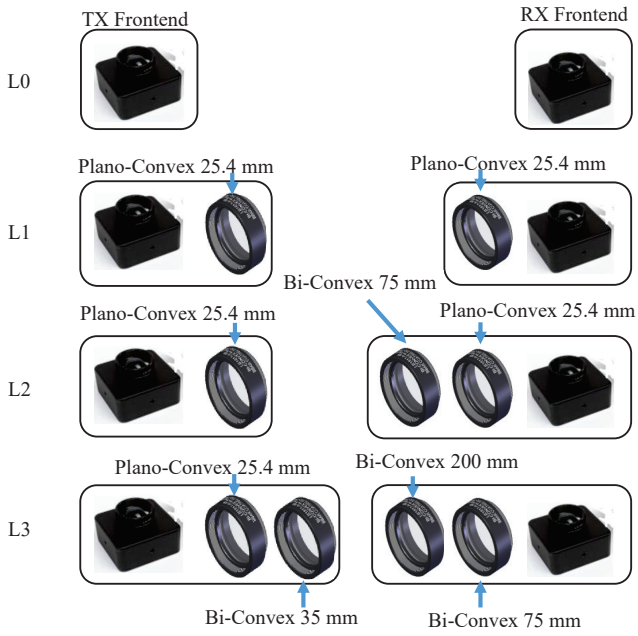

Fig. 2. Lens combinations.

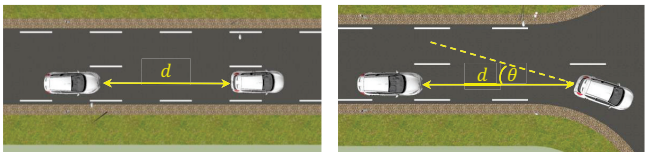

Fig. 3. Scenarios under consideration.

- **L0:** Tx and Rx front-ends are without any lenses
- **L1:** A plano-convex 25.4 mm lens is attached to both Tx and Rx front-ends
- **L2:** It is the same set-up as in L1 with an additional biconvex 75 mm lens as an outer lens at the Rx front-end
- **L3:** The transmitter employs a 25.4 plano-convex followed by an outer 35 mm bi-convex lens at the transmitter while the receiver uses an outer 200 mm bi-convex lens followed by 75 mm bi-convex lens at the receiver

IV. Measurement Results

The measurements were taken in the Ozyegin University campus at the night time and in clear weather conditions. The scenarios under consideration are illustrated in Fig. 3. In the first scenario, we consider two vehicles in the same lane separated by a distance of d. In the second scenario, we assume that the leading car is about to turn with angle θ between transmitter and receiver vehicles.

First, we characterize effective channel coefficient denoted by h_{eff}. We consider the use of Tx and Rx front-ends without any lenses, i.e. L0 case. As defined in (2), the effective channel coefficient includes the effects of both the propagation channel denoted by h_{opt} and system front-end, lenses and filters together represented by h_{sys}. To isolate these two effects, we first measured the received optical power using a power meter (Thorlabs S142C) and determined h_{opt}. In an effort to validate

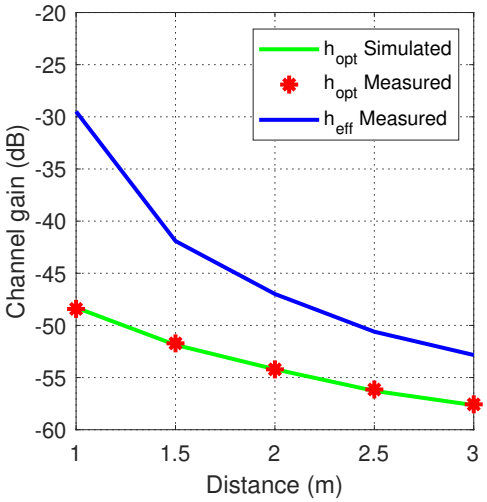

Fig. 4. Comparison of optical propagation channel and effective channel coefficients.

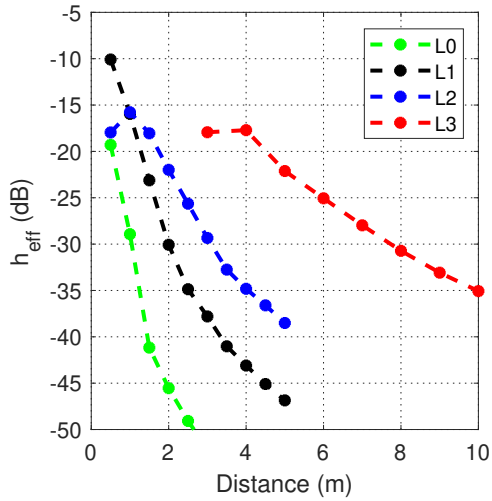

Fig. 5. Effective channel coefficient versus distance for different lens combination at $\theta = 0°$.

this measurement, we further conducted a simulation study using the optical design software OpticStudio® based on the methodology in [15] where the scenario under consideration was modeled as a 3D model and non-sequential ray tracing was used to obtain propagation path loss. The results give a very good match between the measured and simulated h_{opt} values as illustrated in Fig. 4.

In Fig. 5, we present the measured effective channel coefficient $\widehat{h_{eff}}$ with respect to distance for different lens combinations. We consider $\theta = 0°$, i.e., perfect alignment between two vehicles. Curves associated with L1 lens set shows a sharp decay within 5 m while L2 gives a smoother decay because of the additional lens gain. In L2 combination, the additional lens reduces the FOV. Due to the different height (about 15 cm) between both Tx and Rx front-ends, it degrades the system performance at distances below 1 m. In L3 combination, the PD is saturated within the first 3 meters, however it is beneficial for longer distances and transmission span reaches to 10 m.

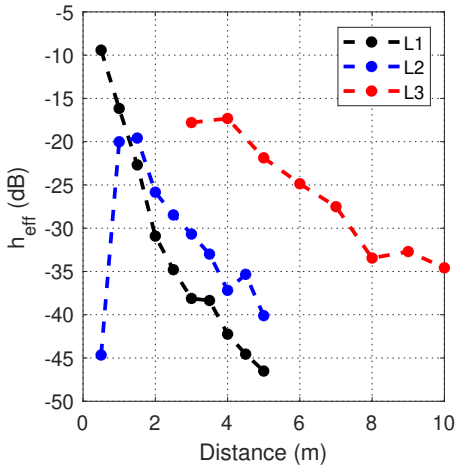

Fig. 6. Effective channel coefficient versus distance for different lens combination at $\theta = 10°$.

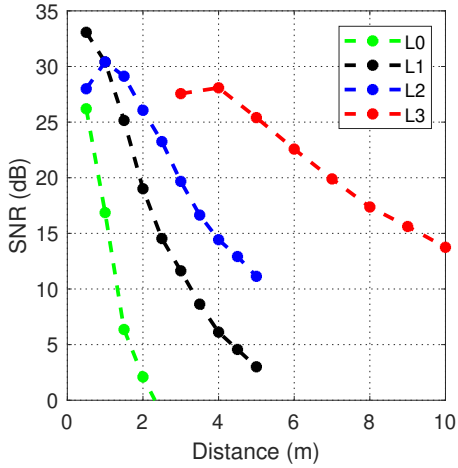

Fig. 7. SNR versus distance for different lens combinations at $\theta = 0°$.

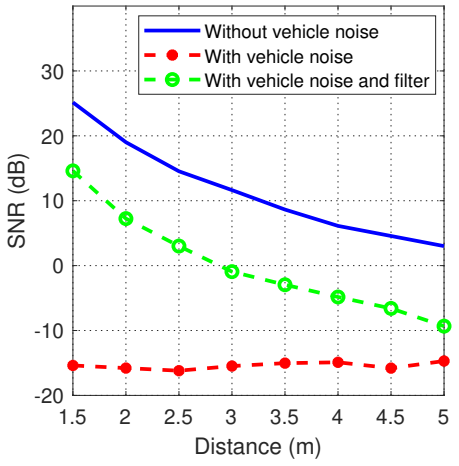

(a)

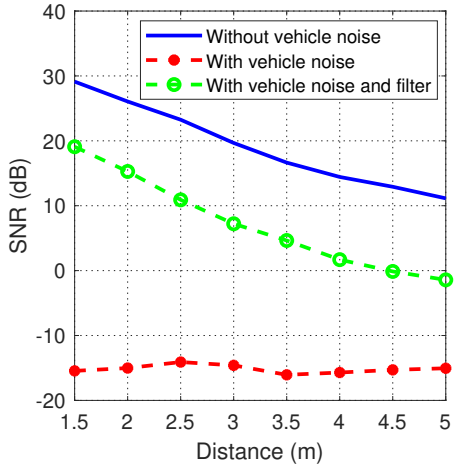

(b)

Fig. 8. Effect of additional noise sources on SNR (a) L1 and (b) L2

In the following, we repeat the above measurements for $\theta = 10°$. As it is observed from Fig. 5 that the effective channel coefficient for the case of L0 falls below 50 dB before the link distance of 2 m. Therefore, we did not include it for the case of $\theta = 10°$. It is observed from Fig. 6 that L1 and L3 follow the same decay curve as in $\theta = 0°$. While L2 starts with a very low value at the distance of 0.5 m, it dramatically increases to peak around 1.5 m before it decays again.

In Fig. 7, we present the received SNR for different lens combinations assuming $\theta = 0°$. We use a transmit power of 0 dB. Based on (4), the noise power is estimated as - 48.27 dB. Replacing these within (6), we obtain estimated SNR result for a specific distance. For L0, the estimated SNR values are 26 dB and 2 dB, respectively, for distances of 0.5 m and 2 m. On the other hand, the SNR for L1 is 30 dB at 1 m and decreases to 4 dB at 5 m. L2 achieves the same SNR at 1 m, but increases to 12 dB at 5 m. In L3, the achievable SNRs are 27, 28 and 14 dB respectively for distances of 3 m, 5 m and 10 m.

In practice, it is possible to experience interference from the other light sources of transmitter vehicle. To demonstrate this effect, we further conducted an experiment keeping open vehicle-daylight halogen lamps and low-beam halogen lamp of the transmitter car. As seen from Fig. 8, additional noises saturate the photodetector. In order to mitigate that effect, a Thorlabs band-pass filter within 450 to 550 nm wavelength is employed. While the filter is able to suppress the undesired wavelengths, it attenuates the received signal power as well. It is observed that there is around 10 dB attenuation of the SNR when bandpass filter is employed.

V. Conclusion

In this paper, we considered a vehicular VLC system with different lens combinations. Using custom-design Tx and Rx front-ends integrated to USPR platforms and mounted on two vehicles, we measured the effective channel coefficient (which includes the effect of both front-ends and propagation channel). Based on estimated channel coefficients and additive noise, we determined SNR values at different link distances for both perfect alignment as well as in the case there is some deviation in the reception angle. For example, assuming perfect alignment, SNR for lens combination L1 decreased

from 30 dB to 4 dB at 1 and 5 m. While for L2, it increased to 12 dB at 5 m much larger than that of L1. For L3, the SNR values were 27, 28 and 14 dB respectively for distances of 3 m, 5 m and 10 m. We further investigated the effect of using daylight and one low-beam signal as an additional noise sources. It was shown that the saturation effect could be dramatically reduced by adding a band pass filter.

REFERENCES

[1] A.Perallos, U. Hernandez-Jayo, I. J. G. Zuazola, and E. Onieva, *Intelligent Transport Systems: Technologies and Applications*. JohnWiley & Sons, 2015.

[2] H. Seo, K. Lee, S. Yasukawa, Y. Peng, and P. Sartori, "Lte evolution for vehicle-to-everything services," *IEEE Communications Magazine*, vol. 54, no. 6, pp. 22–28, June 2016.

[3] M. Uysal, Z. Ghassemlooy, A. Bekkali, A. Kadri, and H. Menouar, "Visible light communication for vehicular networking: Performance study of a v2v system using a measured headlamp beam pattern model," *IEEE Vehicular Technology Magazine*, vol. 10, no. 4, pp. 45–53, Dec 2015.

[4] S. Dimitrov and H. Haas, *Principles of LED Light Communications: Towards Networked Li-Fi*. Cambridge, U.K.: Cambridge Univ. Press, 2015, ch. 2.

[5] P. H. Pathak, X. Feng, P. Hu, and P. Mohapatra, "Visible light communication, networking, and sensing: A survey, potential and challenges," *IEEE Communications Surveys Tutorials*, vol. 17, no. 4, pp. 2047–2077, Fourthquarter 2015.

[6] W. Viriyasitavat, S. Yu, and H. Tsai, "Short paper: Channel model for visible light communications using off-the-shelf scooter taillight," in *2013 IEEE Vehicular Networking Conference*, 2013, pp. 170–173.

[7] M. Karbalayghareh, F. Miramirkhani, H. B. Eldeeb, R. C. Kizilirmak, S. M. Sait, and M. Uysal, "Channel modelling and performance limits of vehicular visible light communication systems," *IEEE Transactions on Vehicular Technology*, pp. 1–1, 2020.

[8] M. Anand and N. Kumar, "New, effective and efficient dimming and modulation technique for visible light communication," in *2014 IEEE 79th Vehicular Technology Conference (VTC Spring)*. IEEE, 2014, pp. 1–4.

[9] A. Cailean, B. Cagneau, L. Chassagne, S. Topsu, Y. Alayli, and J.-M. Blosseville, "Visible light communications: Application to cooperation between vehicles and road infrastructures," in *2012 IEEE Intelligent Vehicles Symposium*. IEEE, 2012, pp. 1055–1059.

[10] Jong-Ho Yoo, Rimhwan Lee, Jun-Kyu Oh, Hyun-Wook Seo, Ju-Young Kim, Hyeon-Cheol Kim, and Sung-Yoon Jung, "Demonstration of vehicular visible light communication based on led headlamp," in *2013 Fifth International Conference on Ubiquitous and Future Networks (ICUFN)*, 2013, pp. 465–467.

[11] R. Yang, X. Jin, M. Jin, and Z. Xu, "Experimental investigation of optical ofdma for vehicular visible light communication," in *2017 European Conference on Optical Communication (ECOC)*, 2017, pp. 1–3.

[12] M. S. Amjad, C. Tebruegge, A. Memedi, S. Kruse, C. Kress, C. Scheytt, and F. Dressler, "An ieee 802.11 compliant sdr-based system for vehicular visible light communications," in *ICC 2019 - 2019 IEEE International Conference on Communications (ICC)*, 2019, pp. 1–6.

[13] M. Y. Abualhoul, E. T. Munoz, and F. Nashashibi, "The use of lane-centering to ensure the visible light communication connectivity for a platoon of autonomous vehicles," in *2018 IEEE International Conference on Vehicular Electronics and Safety (ICVES)*, 2018, pp. 1–6.

[14] R. Corsini, R. Pelliccia, G. Cossu, A. M. Khalid, M. Ghibaudi, M. Petracca, P. Pagano, and E. Ciaramella, "Free space optical communication in the visible bandwidth for v2v safety critical protocols," in *2012 8th International Wireless Communications and Mobile Computing Conference (IWCMC)*, Aug 2012, pp. 1097–1102.

[15] H. B. Eldeeb, F. Miramirkhani, and M. Uysal, "A path loss model for vehicle-to-vehicle visible light communications," in *2019 15th International Conference on Telecommunications (ConTEL)*, July 2019, pp. 1–5.

[16] M. Elamassie, M. Karbalayghareh, F. Miramirkhani, R. C. Kizilirmak, and M. Uysal, "Effect of fog and rain on the performance of vehicular visible light communications," in *2018 IEEE 87th Vehicular Technology Conference (VTC Spring)*, June 2018, pp. 1–6.

[17] B. Aly, M. Elamassie, B. Kebapci, and M. Uysal, "Experimental evaluation of a software defined visible light communication system," in *IEEE ICC 2020 Workshop on Optical Wireless Communications (IEEE ICC'20 Workshop - OWC)*, Dublin, Ireland, Jun. 2020.

[18] R. W. H. Jr., *Introduction to Wireless Digital Communication: A Signal Processing Perspective*. Englewood Cliffs, NJ, USA: Prentice-Hall,, Mar. 2017.

[19] B. Aly, M. Elamassie, M. Uysal, and E. Kınav, "Experimental evaluation of unipolar OFDM VLC system on software defined platform," in *2019 15th International Conference on Telecommunications (ConTEL)*, July 2019, pp. 1–6.

[20] Ettus Research, http://www.ettus.com, [Accessed: May 26, 2020].

[21] LiFi R&D kit, http://www.hyperiontechs.com/li-fi-rd-kit-1/, [Accessed: May 26, 2020].